Surrogate Hamiltonian study of electronic relaxation in the femtosecond laser induced desorption of NO/NiO(100)

Christiane P. Koch,[a] Thorsten Klüner,[b] and Hans-Joachim Freund
Fritz-Haber-Institut der Max-Planck-Gesellschaft, Faradayweg 4-6, 14195 Berlin, Germany

Ronnie Kosloff
Department of Physical Chemistry and The Fritz Haber Research Center, The Hebrew University, Jerusalem 91904, Israel

(Received 11 February 2003; accepted 2 April 2003)

A microscopic model for electronic quenching in the photodesorption of NO from NiO(100) is developed. The quenching is caused by the interaction of the excited adsorbate–substrate complex with electron hole pairs ($O\,2p \rightarrow Ni\,3d$ states) in the surface. The electron hole pairs are described as a bath of two level systems which are characterized by an excitation energy and a dipole charge. The parameters are connected to estimates from photoemission spectroscopy and configuration interaction calculations. Due to the localized electronic structure of NiO a direct optical excitation mechanism can be assumed, and a reliable potential energy surface for the excited state is available. Thus a treatment of *all* steps in the photodesorption event from first principles becomes possible for the first time. The surrogate Hamiltonian method, which allows one to monitor convergence, is employed to calculate the desorption dynamics. Desorption probabilities of the right order of magnitude and velocities in the experimentally observed range are obtained. © *2003 American Institute of Physics.* [DOI: 10.1063/1.1577533]

I. INTRODUCTION

A molecule which is adsorbed on a surface can be detached by thermal or photoexcitation. For chemisorbed molecules, desorption involves the cleavage of a chemical bond, and it represents the simplest case of a chemical reaction. Since molecule and surface degrees of freedom are coupled, energy is transferred from the surface to the molecule and vice versa. The nature of the excitation process reveals itself in the observables of the desorption experiment: Thermal desorption results in the distribution of energy onto all degrees of freedom while for laser induced desorption the excitation of specific quantum states resulting in a nonthermal distribution of energy can be observed. The theoretical description of laser induced desorption must therefore be quantum mechanical and start from first principles. In particular, all aspects of the problem should be treated on the same level of rigor.

The photodesorption process consists of three steps—excitation of the molecule due to the interaction with the laser pulse, relaxation of the excitation energy into the surface, and subsequent desorption. In previous treatments,[1] the emphasis has been placed on the molecular dynamics. It is the goal of this paper to go one step further and also treat the dynamical interaction between molecule and surface on an *ab initio* level. To this end, the surrogate Hamiltonian method[2,3] to model the dissipative quantum dynamics is combined with *ab initio* potential energy surfaces obtained in previous work.[4,5]

Two mechanisms for laser induced desorption based on short-lived electronically excited states have been suggested.[1] The Menzel–Gomer–Redhead (MGR) model[6,7] assumes the electronically excited state to be repulsive, while in a variation of the MGR model going back to Antoniewicz[8] the excited state is bound. In both models, the excitation from the electronic ground to an excited state and the relaxation back to the ground state are modeled as vertical transitions of a classical particle or a quantum mechanical wave packet. If an ensemble of wave packets is considered,[9,10] each wave packet spends a certain residence time on the excited state. Expectation values can then be computed as stochastic averages of the ensemble where the resonance time, i.e., the lifetime of the excited state, enters as a weight. This procedure is usually termed Gadzuk's wave packet jumping. A quantitative theoretical description has to be based on an *ab initio* treatment of the participating potential energy surfaces and excitation and deexcitation mechanisms.

The calculation of reliable potential energy surfaces in general, and for excited states in particular, is still an open problem. However, for NO/NiO(100)[4,5] excited state potentials were obtained on an *ab initio* level. The topology of the representative excited state potential for NO/NiO(100) which was used in the calculations will be discussed in Sec. II B.

Irradiation by nanosecond pulses can well be described by a Franck–Condon transition. The theoretical description of femtosecond experiments, however, requires an improved model since excitation, excited state dynamics, and relaxation all occur on the same time scale. For metals, the two-temperature model[1] has been introduced to describe femtosecond excitation of the surface. The excitation mechanism is assumed to be substrate-mediated, i.e., the pulse generates a cloud of hot electrons which can attach to or scatter from

[a]Electronic mail: koch_c@fhi-berlin.mpg.de
[b]Electronic mail: kluener@fhi-berlin.mpg.de

the adsorbate. On oxides, the substrate is also involved in the excitation process. This can be seen in the linear dependence of the desorption cross section on the laser energy once the laser energy is larger than the band gap.[11] The excitation mechanism can, however, be thought of as direct *within* the substrate–adsorbate complex as will be discussed in Sec. II C. Then the full time-dependence of the pulse enters the theoretical model.

The electronic excitation of the adsorbate is dissipated into the surface due to interaction with surface electrons and holes or phonons. The lifetime of the electronic excitation is extremely short.[12] For metals it is estimated to be $\tau \lesssim 1$ fs while for oxides it is assumed to be somewhat larger, $\tau \approx 20-30$ fs. If the interaction with charge carriers in the surface is seen as the primary cause of relaxation, this difference corresponds to the different density of states in metals and insulators. In both cases the short lifetime leads to the conclusion that the interaction with the surface must be strong.[1] If a fully quantum mechanical description of the problem is desired, an open quantum system approach should be used to describe the relaxation process. The surface electron–hole pairs and phonons are then modeled as environment or bath.

There are two standard approaches to the problem of open quantum systems, perturbation theory and the dynamical semigroup formalism. In both cases, the total Hamiltonian is separated into parts describing the (primary) system and the (secondary) bath, $\hat{\mathbf{H}}_S$ and $\hat{\mathbf{H}}_B$,

$$\hat{\mathbf{H}}_{\mathrm{tot}} = \hat{\mathbf{H}}_S + \hat{\mathbf{H}}_B + \hat{\mathbf{H}}_{SB}. \tag{1}$$

In a perturbation theory treatment,[13,14] the coupling between system and bath, $\hat{\mathbf{H}}_{SB}$, is assumed to be weak. Equations of motion for the reduced density operator, i.e., the density operator of the system $\hat{\boldsymbol{\rho}}_S$, can then be derived which depend upon system operators only. The derivation in a most general sense is done by the projection operator technique.[14,15] The drawback of this reduction is the occurrence of memory effects describing the correlations between system and bath. It is well known, however, that the dynamics of the reduced density operator does not obey complete positivity.[16] This obscures the interpretation of diagonal matrix elements of $\hat{\boldsymbol{\rho}}_S$ as probabilities. The condition of complete positivity together with the Markov assumption is the starting point of the second approach. These two conditions are fulfilled if the Liouville superoperator generating the dynamics of $\hat{\boldsymbol{\rho}}_S$ is of so-called Lindblad form.[17,18] Dissipation is modeled by system operators which have to be chosen semi-phenomenologically.[19]

Both perturbation theory and semigroup formalism lead to an equation of motion for the density operator of the system which needs to be solved. A description based on the system wave function with a more favorable scaling in the numerical solution is also possible. The influence of the bath on the system is then treated as a stochastic force and the method is hence termed the stochastic wave packet or Monte Carlo wave function (MCWF) method.[20–23] The MCWF method was shown to be equivalent to the semigroup formalism.[20–22] For laser induced desorption, the MCWF method is furthermore equivalent to Gadzuk's wave packet jumping if a coordinate-independent relaxation rate is assumed.[24,25]

While the Markov approximation is intrinsic for the semigroup approach, the equation of motion obtained in a perturbation theory approach in general is non-Markovian. Since the solution of integro-differential equations is far from being straightforward, the Markov approximation usually needs to be made. It is, however, not necessarily justified in the case of moderate or strong coupling between system and bath which can be expected for laser induced desorption. Within second-order perturbation theory different approaches exist to treat the memory kernel in the reduced equation of motion. One possibility consists in transforming the integro-differential equation into an algebraic equation by expanding the reduced density operator in a suitable polynomial basis, e.g., Laguerre polynomials.[26] The method is limited, however, to weak field excitation. If the interaction with strong external fields is to be considered, the non-Markovian equation of motion for the system density matrix can be transformed into a set of coupled Markovian equations for the reduced density matrix and auxiliary density matrices which incorporate the memory effects.[27] This method is best suited for high temperature calculations. No further assumptions other than the weak coupling approximation need to be made.[27]

The path integral formalism supplies a different approach to open system quantum mechanics.[28–30] For a linearly coupled bath of harmonic oscillators, the bath variables can analytically be integrated. The effect of the bath is then captured in an influence functional.[28] Non-Markovian effects result in an influence functional containing correlations in time between different paths,[31] i.e., they can in principle be accounted for. However, the numerical evaluation of a multidimensional integral remains computationally challenging despite recent progress.[31] This limits the applications of path integrals to relatively simple model systems. Furthermore, the treatment of time-dependent Hamiltonians is not possible.

The theoretical description of femtosecond laser induced desorption thus poses a dilemma: Strong interaction with the environment excludes perturbation theory. The impossible separation of excitation and relaxation time scales makes non-Markovian effects likely to be important. An anharmonic environment (the electron–hole pairs in the surface), comparatively low temperature, and an explicit time dependence of the Hamiltonian are not well suited for a path-integral approach.

The number of existing theoretical studies is therefore small. The above-mentioned two-temperature model was used in a semigroup treatment for NO/Pt(111).[32,33] The indirect treatment of the pulse in the two-temperature model prolonged the excitation time scale justifying the Markov assumption inherent in the semigroup approach. Another indirect treatment of the excitation process has been applied to CO/Cu(111).[34,35] The surface was treated as stochastic environment leading to an optical potential in the system Hamiltonian. Memory effects were considered to be negligible due to the internal energy transfer in the surface. Direct

optical excitation without further justification has been assumed for $NH_3/Cu(111)$[36] although the excitation is known to be substrate-mediated.[37] The deexcitation was also modeled by an optical potential, i.e., assuming a δ-correlated environment. However, the field is known to affect the dissipation.[38] Since excitation and deexcitation are both caused by electrons in the copper surface, and the time scales of excitation and relaxation are comparable, correlations between excitation and dissipation have to be expected but were not accounted for.

The present paper presents a theoretical study of femtosecond laser induced desorption of NO/NiO(100). This system has been the subject of numerous epxerimental[11,39–41] as well as theoretical studies.[4,42,43] The most prominent feature of the experimental results is a bimodality of the desorption velocity distributions and a coupling of rotational and translational energy for the fast desorption channel.[39] These findings could be explained in terms of the topology of the excited state potential and the excited state dynamics within a two-dimensional jumping wave packet treatment.[42] However, the lifetime of the excited state had to be chosen semiempirically. Furthermore, such a stochastic approach neglects correlations between excitation and relaxation which become important in femtosecond experiments as currently performed. The introduction of femtosecond laser technology requires a theoretical treatment of excitation and deexcitation mechanisms on the same level of rigor. In particular, a microscopic description of the dissipation has not been attempted so far. We therefore combine the information from previous studies[4,11,39,40,42,43] with the surrogate Hamiltonian method[2,3] to develop a model which treats the nuclear dynamics as well as the excitation and relaxation mechanism on the same level of rigor.

The surrogate Hamiltonian is complementary to other approaches to dissipative quantum dynamics which are based on a reduced description of the system. This is particularly interesting in light of the rigorous proof that a reduced dynamics in general does not exist for quantum systems.[44] For the surrogate Hamiltonian the starting point is a description of the total system and bath. This description is approximated in a controlled way yielding a model whose treatment is numerically feasible but whose validity is limited in time. No weak coupling assumption needs to be made, and the coupling constants can be derived from first principles. The environmental modes are described as two level systems (TLS). Such an excitonic bath is particularly well-suited to model the electron–hole pairs in the surface. The interaction with phonons is not likely to play a role: It requires lifetimes at least on the picosecond to nanosecond time scale. The temperature dependence of desorption observables could furthermore be explained purely by initial population of ground vibrational states.[45] The interaction of the excited adsorbate–substrate complex with phonons is therefore neglected. In principle, however, it could be incorporated in the model by employing a second bath.

The treatment of time-dependent fields can be included naturally into the description. Furthermore, the strength of the surrogate Hamiltonian lies in the low temperature regime. Since the focus is on developing a microscopic understanding of the interaction between substrate, adsorbate, and laser pulse, the model will, however, be restricted to one nuclear dimension—the desorption coordinate. Observables of interest are therefore desorption yield and desorption velocities. Once a fully quantum mechanical description of the desorption event including electronic states, excitation, and relaxation mechanisms has been obtained, a generalization to more degrees of freedom is possible. This would allow for calculating furthermore rotational and vibrational distributions. Such a generalization is beyond the scope of the present work which serves as one more step toward a complete quantum description of laser induced desorption.

II. THE SURROGATE HAMILTONIAN METHOD APPLIED TO LASER INDUCED DESORPTION OF NO FROM NIO(100)

When the total system is separated into primary system and secondary bath parts, its Hamiltonian is given by Eq. (1). If in addition the interaction with a laser field is explicitly considered, the Hamiltonian can be written as

$$\hat{\mathbf{H}}_{\mathrm{tot}} = \hat{\mathbf{H}}_S + \hat{\mathbf{H}}_{SF}(t) + \hat{\mathbf{H}}_{SB} + \hat{\mathbf{H}}_{BF}(t) + \hat{\mathbf{H}}_B , \tag{2}$$

where the interaction of the primary system and of the environment with the field is described by $\hat{\mathbf{H}}_{SF}(t)$ and $\hat{\mathbf{H}}_{BF}(t)$, respectively. In the present study, the system Hamiltonian $\hat{\mathbf{H}}_S$ describes the adsorbed NO molecule on a finite part of the NiO surface (cf. Sec. II B), while the remaining part of the surface is modeled as environment or bath $\hat{\mathbf{H}}_B$ (cf. Sec. II D). The effect of this environment on the system is captured in the interaction term $\hat{\mathbf{H}}_{SB}$ (cf. Sec. II E). Before proceeding with the application of the surrogate Hamiltonian to laser induced desorption of NO/NiO(100), the general idea of the method[2,3] is recalled.

A. Brief review of the surrogate Hamiltonian method

In quantum mechanics the effort to solve a problem scales exponentially with the number of degrees of freedom. Except for a few special, analytically solvable cases, Eqs. (1) and (2) therefore state an extremely complicated problem for which approximations are unavoidable. Since the bath degrees of freedom themselves are not interesting, and only their influence on the system is important, the first step of approximation consists in an implicit description of the bath by abstract, representative modes. The core idea of the surrogate Hamiltonian[2] is the truncation of the infinite number of representative bath modes in a well-defined way. This is possible if the modes are chosen such that the ones which interact strongest with the system are always included in the description. This leads to a new, ''surrogate'' Hamiltonian for the total system which generates the time evolution of a ''surrogate'' wave function, $\Psi(Z,\alpha,\sigma_1,\sigma_2,\ldots,\sigma_N)$. Z represents the nuclear coordinate of the system, α the electronic level, and σ_i the bath degrees of freedom. Observables are associated with operators of the primary system. They can be determined from the reduced density operator, i.e., the density operator of the primary system:

$$\hat{\boldsymbol{\rho}}_S(Z,Z',\alpha,\alpha') = \mathrm{tr}_B\{|\Psi(Z,\alpha,\{\sigma_i\})\rangle \times\langle\Psi^*(Z',\alpha',\{\sigma_i'\})|\}, \quad (3)$$

where $\mathrm{tr}_B\{\ \}$ denotes a partial trace over the bath degrees of freedom. The system density operator is thus constructed from the total system–bath wave function while only this wave function is propagated. This *a posteriori* construction of the density operator is different from most other approaches to dissipative quantum dynamics[14,46,47] where the trace over the bath is performed before time propagation, possibly neglecting correlations between system and bath. As a consequence of the surrogate model, all correlations between system and bath which the Hamiltonian allows for are included. Furthermore, since the Schrödinger equation for a wave function is solved, the treatment of time-dependent external fields poses no additional problems.

In the limit of an infinite number of bath modes, the surrogate Hamiltonian is completely equivalent to the original, ''true'' Hamiltonian. Since, at least in principle, the number of modes N can be increased, it is possible to check convergence. The truncation leading to the surrogate Hamiltonian relies on a time-energy uncertainty argument: In a finite time, $t \ll \infty$, the system can only resolve a finite number, $N \ll \infty$, of bath states and not the full density of states. The sampling density in energy of the finite set of bath states is determined by the inverse of the time interval. This argument leads to two observations—the surrogate Hamiltonian is well-suited for the description of ultrashort events, and the number of needed modes increases with the interaction strength between system and bath. Strong and intermediate coupling strengths might therefore pose a computational challenge. From the above-mentioned derivation, it is clear, however, that no weak coupling assumption was needed. In addition, the surrogate Hamiltonian method yields a *controllable* approximation.

The bath is composed of TLS and described by the Hamiltonian

$$\hat{\mathbf{H}}_B = \mathbb{1}_S \otimes \sum_i \varepsilon_i \hat{\boldsymbol{\sigma}}_i^\dagger \hat{\boldsymbol{\sigma}}_i \quad (4)$$

with $\hat{\mathbf{n}}_i = \hat{\boldsymbol{\sigma}}_i^\dagger \hat{\boldsymbol{\sigma}}_i$ the occupation number operator and ε_i the energy of the ith bath mode. For N bath modes the Hilbert space $\mathcal{H}_B$ of the bath has dimension 2^N. This results from a single TLS or spin-$\frac{1}{2}$ being defined on a two-dimensional Hilbert space and the possibility to combine each of the two basis states for all N modes. The dimension of the total Hilbert space $\mathcal{H}_S \otimes \mathcal{H}_B$ is then given by the product of the dimensions of $\mathcal{H}_S$ and 2^N. Obviously, this dimension quickly gets very large when the number of bath modes N is increased. However, considering all 2^N possibilities of combining the bath modes corresponds to considering *all* possible system–bath correlations which might not be necessary. The number of simultaneously allowed excitations can then be restricted. In an extreme case, only single excitations are considered. This reduces the dimension of the total Hilbert space from 2^N to $N+1$. The approximation made is again controllable since the number of simultaneously allowed excitations can be increased. In the present study, the eigenvalues ε_i and eigenstates n_i of the bath were obtained within a microscopic model (cf. Secs. II D and II E). The TLS bath can also be viewed as a low temperature approximation to a harmonic oscillator bath with the possibility of connecting the parameters of the two models.[48–52]

B. The primary system

The Hamiltonian of the primary system, $\hat{\mathbf{H}}_S$, describes two electronic states and one nuclear degree of freedom, $\hat{\mathbf{Z}}$, which is the distance of the molecule from the surface,

$$\hat{\mathbf{H}}_S = \begin{pmatrix} \hat{\mathbf{T}} + V_g(\hat{\mathbf{Z}}) & 0 \\ 0 & \hat{\mathbf{T}} + V_e(\hat{\mathbf{Z}}) \end{pmatrix}. \quad (5)$$

$\hat{\mathbf{T}}$ denotes the kinetic energy operator which is applied in momentum space. Potential energy surfaces $V_{g/e}(\hat{\mathbf{Z}})$ have been constructed by Klüner and co-workers[4,5] in two dimensions—distance from the surface Z and polar angle θ between the NO molecular axis and the surface normal. In the present study the angle is kept fixed at the equilibrium value $\theta = 45°$. The excited state potential has been calculated in a valence configuration interaction (CI) approach for a NO/NiO_5^{8-} cluster embedded in a point charge field.[4,5] The excited state is a charge-transfer state which is characterized by a deep potential well due to Coulomb interaction between NO^- and the positively charged cluster and by a potential minimum at a distance of about 1.5 a.u. smaller than the electronic ground state minimum. The wave packet will therefore be accelerated toward the surface upon excitation and desorption will occur according to the Antoniewicz mechanism.[8]

CI has so far been the only method to obtain excited states for adsorbates on transition metal oxides.[4,53] However, within such an approach based on a finite cluster only relative energies and the topology of the potential energy surface are expected to be reliable. Vertical excitation energies can only be estimated due to orbital relaxation within the cluster and due to extra cluster polarization.[54] Since many excited states are located in the energy range probed by the laser pulse, the field is likely to cause a resonant transition. However, since the topology of these states is very similar,[5] it is possible to select one representative state whose excitation energy coincides with the laser energy.

C. The interaction with the laser field

The Hamiltonian, Eq. (2), includes both direct $[(\hat{\mathbf{H}}_{SF}(t)]$ and substrate-mediated $[\hat{\mathbf{H}}_{BF}(t)]$ excitation of the primary system. However, in the following only direct optical excitation will be considered. For metal surfaces direct optical excitation can be excluded due to the strong quenching of electrons in the conduction band. This situation is different for oxide surfaces which have a considerable band gap. Measurements with different polarizations of the laser pulse found a dependence of the desorption yield on the polarization while the desorption velocities were not influenced.[55] If the excitation is mediated by the substrate,[1] the excitation energy is dissipated into the surface via electron–electron and (secondary) electron–phonon scattering. These multiple

scattering events rule out a symmetry dependence of the excitation. In contrast, a direct excitation is determined by the symmetry of the states involved. The polarization dependence of the desorption yield for NO/NiO(100) favoring *s*-polarized light[55] is compatible with calculated oscillator strengths.[4,5] It therefore supports an electronic excitation mechanism which is determined by optical selection rules, i.e., a direct optical excitation within the adsorbate–substrate complex.

If a direct optical excitation of the adsorbate–substrate complex is assumed, the primary system interacts with the electric field $E(t)$ of the laser pulse which causes an electronic transition,

$$\hat{\mathbf{H}}_{SF}(t)=\begin{pmatrix} 0 & E(t)\hat{\boldsymbol{\mu}}_{\mathrm{tr}}(\hat{\mathbf{Z}}) \\ E^*(t)\hat{\boldsymbol{\mu}}_{\mathrm{tr}}(\hat{\mathbf{Z}}) & 0 \end{pmatrix}. \tag{6}$$

$\hat{\boldsymbol{\mu}}_{\mathrm{tr}}(\hat{\mathbf{Z}})$ is the transition dipole operator depending on the nuclear coordinate. The field $E(t)$ is treated semiclassically, and its spatial dependence is neglected. The shape of the field is assumed to be Gaussian,

$$E(t)=E_0\exp\left(-\frac{(t-t_{\max})^2}{2\sigma_P^2}\right)e^{i\omega_L t}. \tag{7}$$

Since the excitation is taken to be resonant, the laser frequency ω_L coincides with the difference of V_g and V_e at the minimum of the ground state potential. The parameters characterizing the pulse are its frequency ω_L, the intensity E_0 or the pulse fluence which is related to E_0, and the full width half maximum (FWHM) τ_P which is related to the standard deviation σ_P by $\tau_P=2\sigma_P\sqrt{2\ln 2}$. The transition dipole $\hat{\boldsymbol{\mu}}_{\mathrm{tr}}(\hat{\mathbf{Z}})$ can be obtained from the oscillator strength f,

$$f=\tfrac{2}{3}E_{fi}|\mu_{fi}|^2 \tag{8}$$

(in atomic units). f was found to be approximately $f=\exp(-\hat{\mathbf{Z}})$ in the *ab initio* calculations,[4,5] and $E_{fi}\approx 4$ eV $=0.15$ a.u.

D. The electron hole pair bath

The lifetime of the excited state has been estimated as about 15–25 fs, i.e., the charge transfer state is extremely short-lived,[4] but the lifetime is still considerably larger than those estimated for desorption from metal surfaces.[1] Optical deexcitation and interaction with phonons require lifetimes at least on the picosecond to nanosecond time scale and can therefore be excluded as possible relaxation channels. The interaction with phonons is furthermore not likely to play a role since the temperature dependence of desorption observables could be explained purely by initial population of ground state vibrational states.[45] The remaining possible relaxation channel is electronic quenching caused by the interaction with electron hole pairs, i.e., $\mathrm{O}\,2p\rightarrow\mathrm{Ni}\,3d$ charge transfer states in the surface.

The electron hole pairs are described as a TLS bath,

$$\hat{\mathbf{H}}_B=\varepsilon\sum_i \hat{\boldsymbol{\sigma}}_i^+\hat{\boldsymbol{\sigma}}_i+\frac{\eta}{\log(N)}\sum_{ij(\mathrm{NN})}(\hat{\boldsymbol{\sigma}}_i^\dagger\hat{\boldsymbol{\sigma}}_j+\hat{\boldsymbol{\sigma}}_j^\dagger\hat{\boldsymbol{\sigma}}_i), \tag{9}$$

where (NN) stands for nearest neighbor, and $\hat{\boldsymbol{\sigma}}_i^+$, $\hat{\boldsymbol{\sigma}}_i$ are the creation and annihilation operators for the ith TLS, respectively. Equation (9) implies that one electron hole pair located at site i is modeled by the ith TLS. The sites are Ni–O pairs in the lattice between which charge transfer can occur. The first term in Eq. (9) describes the excitation of localized TLS at the sites i. This is motivated by the Ni $3d$ states being in general localized.[56] Delocalization is brought about by the O $2p$ states and introduced into the model by the second term in Eq. (9). This term describes the transport of excitation from one electron hole pair to its nearest neighbors. The bath is hence characterized by two parameters, ε and η. All electron hole pairs are assumed to have identical excitation energy ε. In a molecular orbital picture this is the transition energy from the highest occupied molecular orbital to the lowest unoccupied molecular orbital. η is the interaction strength between nearest-neighbor TLS and leads to a finite width of excitation energy, i.e., an energy band of the bath: If the bath Hamiltonian, Eq. (9), is diagonalized, and N is the number of modes, N energies around ε correspond to single excitations, N energies around 2ε correspond to double excitations, etc. The spread of these eigenvalues around ε is determined by η. The scaling $1/\log(N)$ of the second term in Eq. (9) needs to be introduced to make the procedure convergent, i.e., to have the spread of energies around ε independent of the number of bath modes N. It results from the topology of the problem, i.e., from the mapping of two dimensions of the bath onto one (cf. the Appendix). The interaction itself does not scale with N since the bath modes are localized.[48] To summarize, the parameter ε can be viewed as the center of the bath energy band while η determines its width.

Equation (9) represents an abstraction from the complicated electronic structure of actual $\mathrm{O}\,2p\rightarrow\mathrm{Ni}\,3d$ charge transfer states in the surface. Therefore, it should be possible to estimate reasonable values of ε and η from either electron spectroscopy or electronic structure theory. From experiment[57,58] as well as theory,[54,59] the band gap of NiO is known to be about 4 eV with some surface states corresponding to $d\rightarrow d$ excitations of nickel at lower energies. The width of the energy band of single electronic excitations was found to be about 10 eV. However, laser energies between 3.2 and 6.4 eV[41] do not probe the whole energy band. If ε and η are chosen in direct correspondence to the electron energy loss spectroscopy data and CI calculations, modes with energy higher than those probed by the laser are included. However, while these modes exist, they do not contribute to the quenching dynamics. An opimal choice will therefore put as many modes as possible into the physically relevant range, i.e., the energy range set by the laser energy. A thorough discussion of the role of ε and η will be given in Secs. III B–III D.

E. A microscopic model for the system–bath interaction

The interaction of the electron hole pairs with the NO^- like intermediate leads to quenching of electronic excitation of the primary system. The electron hole pairs can be viewed as dipoles, and the laser excitation creates a nonzero transi-

tion dipole in the system. The interaction is therefore modeled as dipole–dipole interaction which assumes that the electric field can be described classically and that the system dipole is in the far field of the bath dipoles. However, compared to the simplification of the O $2p \rightarrow$ Ni $3d$ charge transfer states to TLS, these additional approximations are expected to be negligible. The $\hat{\mathbf{V}}_i$ in the interaction Hamiltonian,

$$\hat{\mathbf{H}}_{SB} = \begin{pmatrix} 0 & 1 \\ 1 & 0 \end{pmatrix} \otimes \sum_i \hat{\mathbf{V}}_i (\hat{\boldsymbol{\sigma}}_i^\dagger + \hat{\boldsymbol{\sigma}}_i), \tag{10}$$

are then given by the scalar product of the system's transition dipole, $\hat{\vec{\boldsymbol{\mu}}}_S$, and the electric field of the bath dipoles, $\vec{E}_i$:

$$\hat{\mathbf{V}}_i = \hat{\vec{\boldsymbol{\mu}}}_S \cdot \vec{E}_i = \frac{\hat{\vec{\boldsymbol{\mu}}}_S \cdot \hat{\vec{\boldsymbol{\mu}}}_i}{|\hat{\vec{\mathbf{r}}}_i|^3} - 3 \frac{(\hat{\vec{\boldsymbol{\mu}}}_S \cdot \hat{\vec{\mathbf{r}}}_i)(\hat{\vec{\boldsymbol{\mu}}}_i \cdot \hat{\vec{\mathbf{r}}}_i)}{|\hat{\vec{\mathbf{r}}}_i|^5}. \tag{11}$$

$|\hat{\vec{\mathbf{r}}}_i|$ is the distance of the ith bath dipole from the system dipole. Note that the $\hat{\mathbf{V}}_i$ are operators in the Hilbert space of the system. Taking into account the expectation value of the transition dipole instead of the operator $\hat{\vec{\boldsymbol{\mu}}}_S$ in Eq. (11) corresponds to a time-dependent self-consistent field (TD-SCF) approach.[34] It introduces the fast time dependence of the transition dipole into the Hamiltonian. Since evaluation of the operator expressions poses no difficulty when using the grid representation, Eq. (11) was implemented using the operators and not expectation values. The bath dipoles are assumed to be located at the center of charge in between a nickel and an oxygen atom. The system dipole is located in between the nickel atom and the NO molecule. Evaluating the scalar products then leads to

$$V_i(\hat{\mathbf{Z}}) = \pm \frac{q a_0 \mu_{\mathrm{tr}}(\hat{\mathbf{Z}})}{\left(\left(\frac{1}{2}(\hat{\mathbf{Z}} + a_0) + m a_0 \right)^2 + n^2 a_0^2 \right)^{3/2}} \mp 3 \frac{q a_0 \mu_{\mathrm{tr}}(\hat{\mathbf{Z}}) \hat{\mathbf{Z}}^2}{\left(\left(\frac{1}{2}(\hat{\mathbf{Z}} + a_0) + m a_0 \right)^2 + n^2 a_0^2 \right)^{5/2}}, \tag{12}$$

where a_0 is the distance between the Ni and O atoms, i.e., half the lattice constant ($2a_0 = 3.93$ Å), and n, $m \in \mathbb{N}$. n labels the sites within the surface (horizontal distance) while m labels the layers (vertical distance, cf. the Appendix). If a one-dimensional primary system is considered, i.e., the tilt angle of NO versus the surface normal is neglected, only the bath dipoles parallel to the surface normal contribute to the interaction. The only parameter in Eq. (12) and therefore in the interaction Hamiltonian $\hat{\mathbf{H}}_{SB}$ is the dipole charge q characterizing the completeness of charge transfer between a nickel and an oxygen atom. An estimate of q is known from *ab initio* calculations.[60] The role of q will be discussed in Sec. III E.

F. Dynamics and observables

The initial state is taken to be the vibrational ground state of the electronic ground state potential. This corresponds to a factorizing initial state at zero temperature in density matrix formalism, i.e., no initial correlations between system and bath are considered. Due to the large band gap of about 4 eV in NiO, no electron hole pairs are thermally excited at time $t = 0$. Hence it is justified to neglect initial correlations between system and bath.

Since a direct excitation mechanism is assumed, the laser pulse transfers population from the electronic ground to the electronically excited state around the Franck-Condon point. The partial wave packets on the electronically excited state start to travel toward smaller distances Z. Due to the interaction with the bath, population is continuously transferred to the electronic ground state. The process is enhanced when the energy of a bath mode matches the potential difference $\Delta V(Z)$. In principle, while both electronic quenching and electronic excitation of the system are possible, the latter is much less probable. This becomes obvious when using the rotating wave approximation (RWA) and moving to the rotating frame. Then the bath creation operators couple only to the electronic annihilator of the system, and the bath annihilators couple only to the electronic creation operator of the system. Electronic excitation of the system can therefore only occur after electronic quenching with the associated creation of bath excitations. The validity of the RWA has been thoroughly checked. The population which has been transferred to the electronic ground state will either be trapped in the potential well though vibrationally excited, or it has gained enough kinetic energy to leave the potential well of the ground state and to desorb. The wave packet is propagated on the electronic ground state until the trapped and the desorbing parts are well separated and the observables in the asymptotic region are converged. The grid switching method proposed by Heather and Metiu is employed.[61]

The convergence of the surrogate Hamiltonian with respect to the propagation time is limited due to recurrences in the bath. Since the bath Hamiltonian is finite, energy transferred from the system to the bath will eventually be reflected and transferred back to the system. At this point (called t_S), the simulation should be stopped and the number of bath modes needs to be increased. In the simulations, t_S can be determined by two criteria, the population backflow and the bath distance criteria. For the first, the population of the zeroth mode corresponding to all TLS being deexcited is monitored. If it increases, population and energy is transferred from the bath back into the system. For the latter, the average distance of the excitation in the bath is calculated. This is possible since every bath mode is connected with a NiO lattice position. A reflection of the excitation at the boundary due to the finite size of the bath leads to a decrease in the bath distance.

Within the convergence time of the surrogate Hamiltonian it is not possible to obtain converged expectation values in the asymptotic region $[V_g(Z) \approx 0]$ which can be compared to observables of laser induced desorption experiments. However, the surrogate Hamiltonian is needed only to describe electronic quenching, it is not necessary to describe the nuclear motion on the electronic ground state leading to a separation of the wave packet into a trapped and a desorbing part: If the decay of the electronic excitation is

fast, the quenching happens on a much shorter time scale (fs) than the nuclear motion in the ground state (ps), and the two phenomena can be separated.

After the interaction has been switched off at time t_S the 2^N ground state wave packets can be propagated until the observables in the asymptotic region are converged. If the wave packet is still comparatively localized, it is, however, more efficient to construct the ground state density matrix $\hat{\boldsymbol{\rho}}_S$ of the system by tracing over the bath. Since no further dissipative processes are included in the description, the time evolution of this reduced density matrix is unitary. Therefore, if $\hat{\boldsymbol{\rho}}_S$ is diagonalized,

$$\rho_S(Z,Z';t)=\hat{\mathbf{U}}^{+}\hat{\mathbf{P}}\hat{\mathbf{U}}=\sum_k p_k|\psi_k(Z;t)\rangle\langle\psi_k(Z';t)|, \quad (13)$$

no further mixing of the wave functions $|\psi_k(Z)\rangle$ will occur during the time propagation. More than one eigenvalue p_k will be nonzero since the wave packet created by electronic quenching and nuclear dynamics is a mixed state. But the number of p_k which contribute significantly in the sum in Eq. (13) is small (usually between 15 and 20 in the examples presented in the following). Expectation values can be constructed as $A(t)=\Sigma_k p_k\langle\psi_k(t)|\hat{\mathbf{A}}|\psi_k(t)\rangle$. The computational savings depend on the number of modes N and can reach several orders of magnitude for large N.

The observables in laser desorption experiments of NO/NiO(100) have been the desorption cross section which is related to the desorption probability and the quantum state resolved velocity of the desorbing molecules.[11,39,40] The desorption probability is obtained by weighting the population in the asymptotic region by the excitation probability. In a one-dimensional model, only average velocity distributions can be observed. The velocity distribution corresponds to the probability density of the wave packet in the asymptotic region in momentum representation.

III. RESULTS AND DISCUSSION

A. Convergence behavior

The time interval for which propagation with the surrogate Hamiltonian gives converged results depends on the number of bath modes N. This interval can be prolonged by increasing the number of bath modes. On the other hand, the convergence of observables with respect to N can be checked. Figure 1 shows the population (left), coordinate (top right), and momentum (bottom right) expectation values on the electronically excited state for $N=35,45,55$. Furthermore, for $N=35$ and for $N=45$, one and two simultaneously allowed excitations (dotted and solid curves) are compared. The curves are indistinguishable, i.e., it is possible to restrict simultaneously allowed excitations to one. This is not surprising, since the energy of double excitations is much higher than the laser energy. Only single excitations have energies in the right range to accept excitation energy from the system and thus can be effective in the quenching. Exponential decay of population can be observed after excitation by the laser pulse (Fig. 1 left), while the wave packet is accelerated toward the surface (Fig. 1 top right). The observables can be considered converged up to about 27 fs for $N=35$, 40 fs for $N=45$, and 60 fs for $N=55$. The convergence time t_c is somewhat smaller than the total length t_S of the curves in Fig. 1 since the interaction with the bath is switched off when recurrences reach the zeroth spinor component. By this time the energy reflected at the boundary of the finite system has already passed through the bath modes. The exponential decay of excited state population within the convergence interval can be fitted to obtain decay rates or lifetimes. Decay rates versus the number of bath modes are plotted in Fig. 2, top panel, while the quality of exponential fit characterized by the correlation coefficient is shown in the bottom panel. Two different values of dipole strength q characterizing the strength of interaction between system and bath (cf. Sec. III E) have been used. The decay rates (lifetimes) saturate at about 0.04 fs^{-1} (25 fs) for $q=0.10$ and 0.075 fs^{-1} (13 fs) for $q=0.14$. The correlation coefficient fluctuates between 0.9980 and 0.9995 showing a good agreement between data and exponential fit.

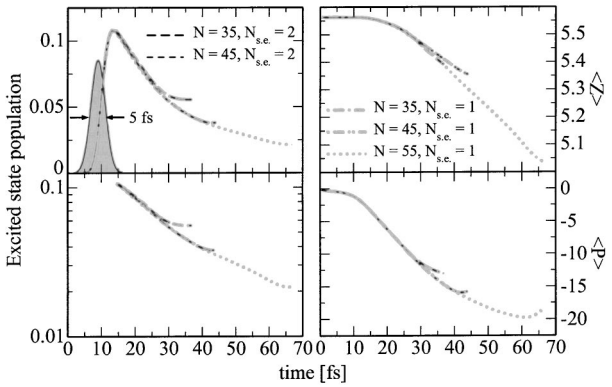

FIG. 1. The excited state population vs time is shown on the left, on a linear (top) and logarithmic scale (bottom). The expectation value of distance (top) and momentum (bottom) of the wave packet on the excited state vs time are shown on the right. Increasing the number of modes N prolongs the convergence time. The number of simultaneously allowed excitations can be restricted to 1 since the black and gray curves are identical. The parameters are $\varepsilon=4.0$ eV, $\eta=2.0$ eV, $q=0.1$, $\omega_L=3.7$ eV.

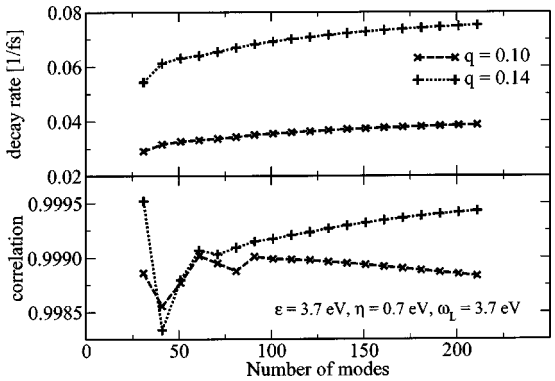

FIG. 2. The excited state decay rate obtained from exponential fit (top) and the correlation coefficient of exponential fit (bottom) are plotted vs the number of bath modes N. The decay rate reaches saturation when increasing N, while the correlation fluctuates in a range close to one.

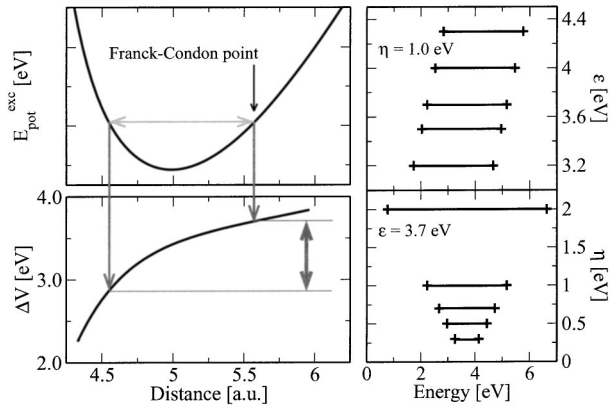

FIG. 3. The range of bath eigenenergies needs to match the difference potential ΔV for quenching to be efficient (left). It is determined by the bath parameters ε and η (right). The difference potential is fixed by assuming resonant excitation at the Franck–Condon point with a laser energy of 3.7 eV.

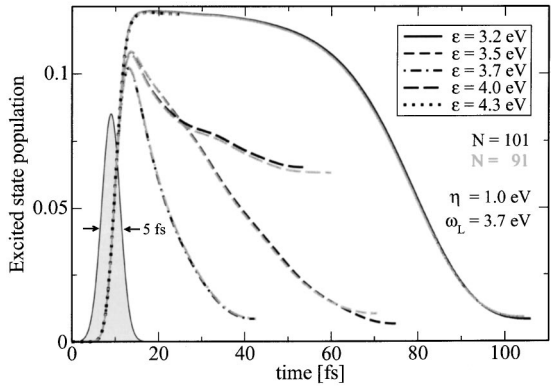

FIG. 4. Dependence of excited state population vs time on the TLS energy ε: If ε and therefore the center of the bath energy band is close to the system resonance fixed by the laser energy ω_L (the dashed curves) the decay of excited state population is exponential, and the choice of ε determines convergence. If the bath energies are larger than the system resonance (dotted curve), the system cannot give energy to the bath and no decay is observed. For bath energies smaller than the system resonance (solid curve), the wave packet needs to travel to a region where the bath energies match the potential difference before decay can occur (see the text for further explanation). N indicates the number of bath modes.

B. Role of center of bath energies for the quenching dynamics

The TLS bath describes electron hole pairs in the surface which cause the quenching of electronic excitation. It is characterized by the two parameters ε and η in Eq. (9), the TLS energy and the nearest-neighbor interaction strength. These parameters are related to the center and width of the energy ''band'' of the bath. Figure 3 shows the range of bath eigenenergies for different values of these parameters on the right. Only single excitations are considered, i.e., the number of simultaneously allowed excitations of the bath is restricted to one. Double excitations would lead to a second bath energy band at larger energies. The left of Fig. 3 displays the excited state potential and the difference potential, $\Delta V(Z) = V_e(Z) - V_g(Z)$. The Franck–Condon point indicated in Fig. 3 determines the classical turning points for the wave packet motion on the excited state (light gray arrow). The values of the difference potential ΔV in between the classical turning points specify the range of bath energies relevant for quenching (bold dark gray). Bath modes with energies within this range can accept energy from or give energy to the system causing a transition between electronic ground and excited state. The bath parameters should therefore be chosen to obtain the best possible convergence of observables with respect to the number of modes ($\varepsilon \approx 3.7-4.0$ eV and $\eta \approx 0.7-1.0$ eV, cf. Figs. 4 and 5). Many electron hole pairs with energies much higher than the laser energy exist[58] but they are not needed. This explains why double, triple, etc., excitations can be neglected in the dynamics.

Figure 4 shows the influence of the TLS energy ε on the excited state dynamics. If ε is considerably larger than the laser energy, the range of bath eigenenergies does not match the values of the difference potential between the classical turning points. The TLS therefore cannot accept energy from the system, and hence no decay of excited state population is observed (dotted curve in Fig. 4). For ε considerably smaller than the laser energy, there are no matching bath modes close to the Franck–Condon point. However, as the wave packet travels toward smaller distances, the value of the difference potential is decreased (cf. Fig. 3), bath energies in the right range are found, and decay of excited state population may be observed with some delay (solid curve in Fig. 4). For intermediate values of ε, the excited state population decays exponentially. Exponential decay corresponds to a constant relaxation rate and allows for a comparison of the surrogate Hamiltonian method with the jumping wave packet approach according to Gadzuk.[5,42] The specific value of ε determines convergence as can be seen from comparison of the black and gray lines (101 and 91 bath modes, respectively) and from Table I. An optimal choice places ε close to the laser energy. This is reasonable also from a physical point of view.

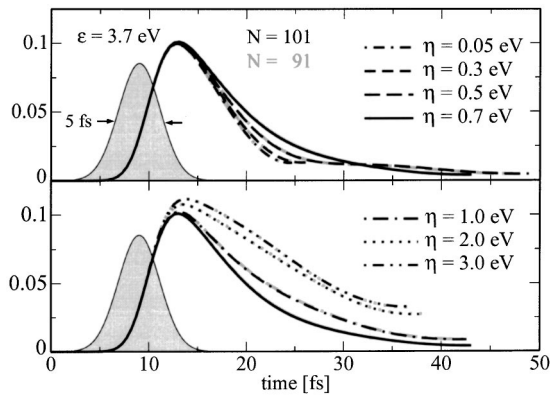

FIG. 5. Dependence of excited state population vs time on nearest-neighbor interaction strength η: For small η (0.05 and 0.3 eV) there is no transport of relaxed population out of the interaction region, the convergence time is very short and cannot be improved by increasing the number of modes N. Increasing η (0.5 eV) leads to transport, however on a time scale larger than the interaction with the system. For $\eta \geqslant 0.7$ eV, the transport is efficient, and exponential decay of excited state population is observed (curves in the bottom panel). Large η causes less quenching of excitation during the interaction of the system with the pulse, and hence a larger maximum population of the excited state.

TABLE I. The quality of exponential fit for the decaying part of the excited state population with TLS energy ε varied is given by the correlation coefficient. The best fit is obtained for $\varepsilon=\omega_L=3.7$ eV. In this case, the quenching is also most efficient (largest decay rate).

ε	Decay rate (1/fs) ($N=101$)	Decay rate (1/fs) ($N=91$)	Correlation of fit ($N=101$)	Correlation of fit ($N=91$)
3.5	0.050	0.046	0.988	0.991
3.7	0.096	0.095	0.997	0.998
4.0	0.011	0.010	0.977	0.967

Since the laser pulse induces an electronic transition in the nickel oxide surface, its energy needs to be equal to or larger than the band gap to which ε is related.

C. Role of the nearest-neighbor interaction for the quenching dynamics

The dependence of excited state population on the nearest-neighbor interaction strength η of the TLS is shown in Fig. 5. Since the dipole–dipole interaction exhibits a $1/Z^3$ dependence, the system interacts only with electron hole pairs which are very close to the NO molecule. To transport the excitation away from this interaction region, the nearest-neighbor coupling between electron hole pairs is needed. If η is very small (0.05 and 0.3 eV in Fig. 5), the excitation cannot be given to TLS outside the interaction region, and the convergence time is determined by saturation of the few TLS close to the primary system. In this case, increasing the number of modes cannot prolong the convergence time. When η is increased, transport sets in leading to a longer convergence time, to slower decay, and to a dependence on the number of modes. Furthermore, the quenching of excitation during interaction of the system with the pulse is less efficient, hence the maximum population of the excited state is increased for larger η (cf. Fig. 5, lower panel). The excited state population decays exponentially—independent of the value of η with the exception of $\eta=0.5$ eV. The decay rates obtained from an exponential fit of the excited state population versus time (Fig. 5) are plotted versus the number of modes in the upper panel of Fig. 6, while the lower panel shows the goodness of the exponential fit characterized by the correlation coefficient. The decay rate is decreased for increasing nearest-neighbor interaction. This can be understood from the following considerations: η determines how quickly relaxed population is transported away from the primary system, but also from TLS close to the primary system. The interaction energy, i.e., the expectation value of the interaction Hamiltonian, Eq. (10), depends on the population of the primary system and of the bath modes close to it. If population is removed from these bath modes, the interaction energy is decreased and the decay becomes slower. If more electron hole pairs are excited close to the NO molecule, the decay becomes faster.

The same argument explains the increase of the maximum excited state population, i.e., decrease of quenching during the interaction with the laser pulse. Since the time scale of this interaction is shorter than that of relaxation (the laser FWHM was chosen as 5 fs), the effect becomes visible only for large η (cf. Fig. 5, right). The correlation coefficients of the exponential fit lie within the interval [0.99,1.0] with the exception of $\eta=0.5$ eV (Fig. 6, bottom). If the data for $\eta=0.5$ eV is fitted only up to 25 fs, its correlation coefficient also lies within [0.99,1.0]. A similar behavior is found for $\eta=0.6$ eV, while the data for $\eta=0.4$ eV is similar to the one with $\eta=0.3$ eV. Thus, variation of η does not change the decay of excited state population qualitatively. This is different from the role of the TLS energy ε (cf. Fig. 4). However, since ε shifts the position of bath eigenenergies while η changes only their width (cf. Fig. 3), this is not surprising.

The considerations have so far only been numerical and suggest an optimal choice of about 0.7–1.0 eV for η. However, an upper limit to the nearest-neighbor interaction strength is also set by the physics of the NO/NiO(100) system: The lowest states are surface states in the optical band gap at about 2.7 eV.[57] These are not charge transfer states, but Ni $d\rightarrow d$ excitations. The charge transfer states lie energetically above the band gap. Therefore no bath modes with energies much below 3.5 eV need to be considered. Of course, if the TLS energy ε is shifted, η should be adjusted to result in a reasonable smallest bath eigenenergy. Accordingly, the optimal choice of bath parameters leading to best possible convergence of expectation values with respect to the number of bath modes is a combination of TLS energy ε and nearest-neighbor interaction strength η. In the following, $\varepsilon=3.7$ eV and $\eta=0.7$ eV were used.

D. Asymptotic observables

So far it has been shown that converged observables related to the excited state dynamics can be obtained. While the excited state dynamics are crucial for the outcome of a laser desorption experiment, they are not directly accessible in a single pulse experiment. Instead, the desorption yield and the state resolved velocity of desorbing molecules are measured, i.e., observables in the asymptotic region. Due to the Antoniewicz-type mechanism of desorption, the

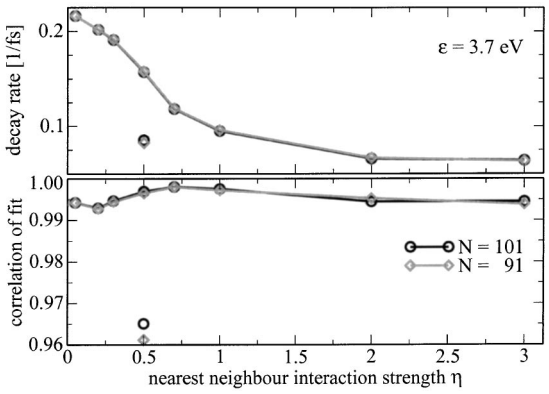

FIG. 6. The decay rates of excited state population which were obtained from an exponential fit of the data shown in Fig. 5 are plotted vs nearest-neighbor interaction strength η (upper panel). It decreases for larger values of η. The goodness of exponential fit is more or less independent of η (lower panel). Two values for the decay rate and the correlation coefficient are plotted for $\eta=0.5$ eV, once the data of the whole range shown in Fig. 5 and once only values of excited state population up to 25 fs were used in fitting.

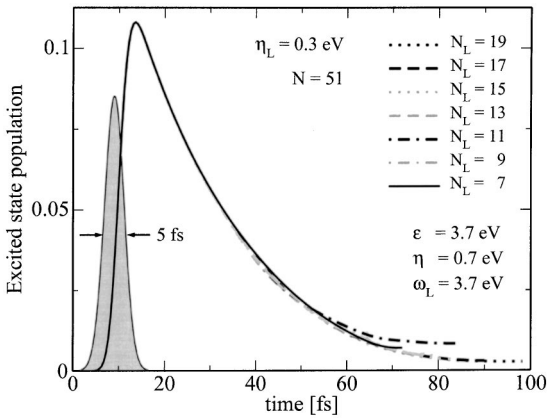

FIG. 7. The population of the excited state vs time. The coupling between electronic states is switched off when recurrences occur, therefore the graph lengths indicate the convergence time.

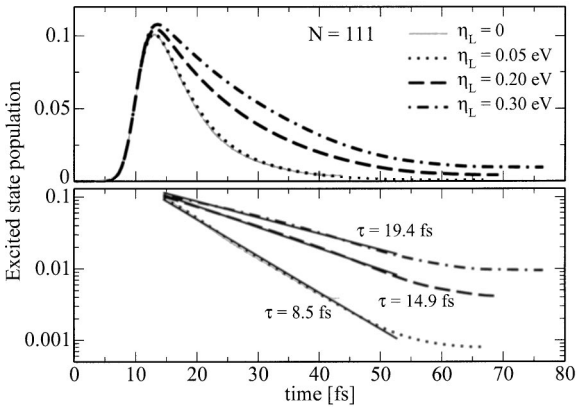

FIG. 8. Increasing the interlayer coupling leads to a slower decay due to faster transport of relaxed population away from the interaction region (parameters as in Fig. 7, but $N_L=5$).

asymptotic observables are detemined by partial wave packets which stay on the excited state for a comparatively long time. In this case, the partial wave packets end up high on the repulsive part of the ground state potential after the electronic quenching. They can then gain enough kinetic energy to leave the potential well and reach the asymptotic region. The convergence of the surrogate Hamiltonian with respect to the number of modes is limited in time. It is therefore comparatively easy to obtain converged excited state dynamics, while it turned out to be more difficult to obtain converged asymptotic observables.

Two strategies can be employed to reach convergence of the asymptotic observables. Either the number of bath modes, N, or the number of layers in the surface, N_L (cf. the Appendix), can be increased. An increase in the number of bath modes, N, enlarges the size of the bath horizontally, and more layers in the surface allow for vertical transport, i.e., transport into the surface. While both processes are equally likely for nickel oxide, they are not treated on the same footing in the model. This is discussed in more detail in the Appendix.

Considering several surface layers indeed leads to a longer convergence time (cf. Fig. 7). The treatment of more than one layer of dipoles introduces a new parameter into the model, the coupling between layers, η_L. Its influence on the excited state dynamics is shown in Fig. 8. A small value of the interlayer coupling (0.0 and 0.05 eV in Fig. 8) does not change the lifetime of the excited state. Increasing the value of η_L leads to slower decay of the electronic excitation (0.2 and 0.3 eV in Fig. 8). This can be understood by an argument similar to the one explaining the dependence of the lifetime on the nearest-neighbor interaction η. The strength of the system–bath interaction depends on the excited state population of the system and on the population of bath modes close to the system. An increase of η_L results in quicker transport of excitation from bath modes close to the system to bath modes further away. Thus the system–bath interaction becomes weaker and the lifetime longer.

As a consequence of the slower decay, increasing the interlayer coupling η_L leads to a larger desorption probability (cf. Fig. 9). While the nearest-neighbor interaction η, i.e., the intralayer coupling, has been directly related to the electronic structure of the system, such a connection has so far not been given for the interlayer coupling, η_L. However, since in the NiO surface the transport of excitation is equally likely horizontally as well as vertically, it is reasonable to assume that η_L should be of the same order of magnitude as η. On the other hand, η_L is related to the convergence properties of the model. This means that there exists an optimal value for which the largest convergence time for a given number of modes and a given number of layers is obtained. If η_L is small, an increase in the number of layers, i.e., an increase of the vertical bath size, will not result in a larger convergence time. In this case, the excitation hits the horizontal boundary of the bath before reaching the vertical limit. For large values of η_L the opposite is true: The vertical is reached before the horizontal boundary. The best convergence is achieved when at the same time both boundaries are reached. The optimal choice of η_L therefore depends on the number of bath modes and the number of layers.

For the parameters investigated, up to 21 layers with $N \leqslant 51$ and up to 13 layers with $N \leqslant 101$ bath modes in each layer were considered. The maximum convergence time was about 90 fs. This was enough to obtain converged desorption

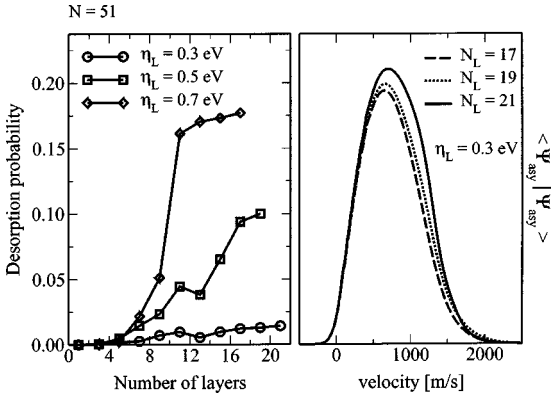

FIG. 9. Increasing the number of layers leads to converged desorption probabilities (left) and velocity distributions (right). The interlayer coupling η_L influences the lifetime of the excited state and therefore also the desorption probability (parameters as in Figs. 7 and 8).

probabilities and velocities (cf. Fig. 9). Desorption probabilities between 1% and 20% were obtained. This is compatible with estimates from experiment.[9,11,62] Furthermore, the velocities are found to be in the experimentally observed range between 0 and 2000 m/s.[39]

The population of the excited state was decreased from its maximum value of about 0.11 to about 0.005 (at best 0.0034 shown in Fig. 7). This means that about 0.5% of the density was left out when the bath was switched off. While this number is small in absolute value, it might be a considerable portion of the desorbing part. The desorption probability is obtained by weighting the norm in the asymptotic region by the excitation probability. One may assume that all or a substantial part of the neglected density desorbs since the coordinate expectation value approaches the value of the classical turning point. In case of a sudden electronic transition much of the kinetic energy would be gained by the wave packet. Weighting the value of 0.5% with the excitation probability results in a possible increase of the desorption probability by 5%. While this is on the same order of magnitude as the desorption probability itself, it is still well within the uncertainty of the experimental estimate.

The second strategy to increase the convergence time consists in increasing the number of bath modes, N, within one layer. A peculiarity is then observed: Above a certain number, N^*, of bath modes a further increase does not result in a prolongation of the convergence time. The exact value of N^* depends on the parameters, in particular on the dipole strength, q, which determines the system–bath interaction strength and hence the convergence. For numbers of modes larger than N^*, the two criteria to monitor recurrences in the bath lead to different convergence times t_S, while for small N the t_S are more or less equivalent. This means that for $N>N^*$, the finite boundary does not seem to be reached when population backflow is observed. A possible interpretation of this phenomenon consists in a polarization of the bath dipoles which interact with the system leading to the backflow of population. Both criteria rely on expectation values, i.e., averages. They can therefore both only give an estimate of the time at which recurrences occur. In addition to the bath distance, also its variance has been examined as switch-off criterion, but no differences could be observed.

A comparison of the two criteria is shown in Fig. 10. Due to the structure of the interaction operator in the RWA, the population backflow can be observed directly by an increase in the excited state population (cf. the upper left panel of Fig. 10). In spite of the backflow of population into the system, Fig. 10 shows that the switch-off criterion employing the distance of the bath is reasonable: The curves of excited state population overlap for an increasing number of bath modes for a time considerably longer than the convergence time given by the population backflow criterion (indicated by the black arrow in Fig. 10). The two switch-off criteria lead to different desorption probabilities (cf. the lower left panel of Fig. 10) owing to the different times the wave packet spent on the excited state. The different times spent on the excited state furthermore result in different velocity distributions (cf. the right panel of Fig. 10). In the case of the bath distance switch-off criterion (gray curves in Fig. 10), the

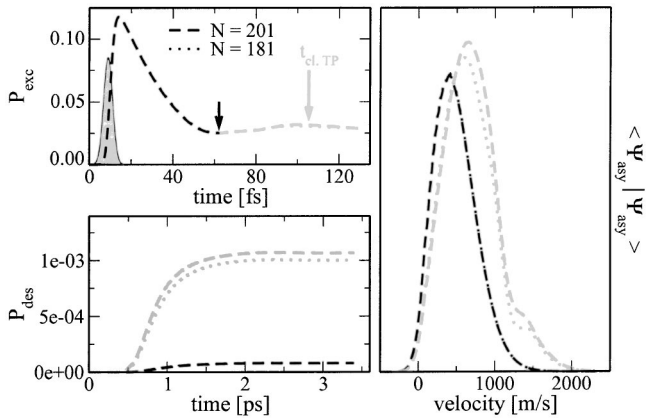

FIG. 10. If the distance of the bath excitation (gray) is used as convergence criterion instead of the population of the system (black), longer convergence times t_S can be obtained (indicated by the black arrow). The time the wave packet spent on the excited state is crucial for both the desorption probability (bottom left) and the shape of the velocity distributions (right, scaled for comparison). The second peak in the velocity distribution can be related to the passage of the classical turning point of the excited state potential (indicated by gray arrow) which has only occurred for the gray curves with $N=181$ and $N=201$. The top left shows the population of the excited state with the pulse (not to scale) indicated (parameters as in the previous figures, but $N_L=1$).

propagation on the excited state continued sufficiently long to pass the classical turning point. Therefore an interference can be observed in the velocity distribution. The interference results from different pathways of partial wave packets which have reached the asymptotic region. It is a *coherent* phenomenon which cannot be observed within a one-dimensional stochastic wave function approach.

This point is clarified by Fig. 11, which shows the excited state population versus time and velocity distributions for a different number of bath modes N. For all three cases in Fig. 11, the switch-off criterion employing the bath distance has been used. For $N=161$ bath modes (gray curves in Fig. 11), the propagation with both electronic states had to be switched off before the classical turning point was reached. The corresponding velocity distribution therefore shows only

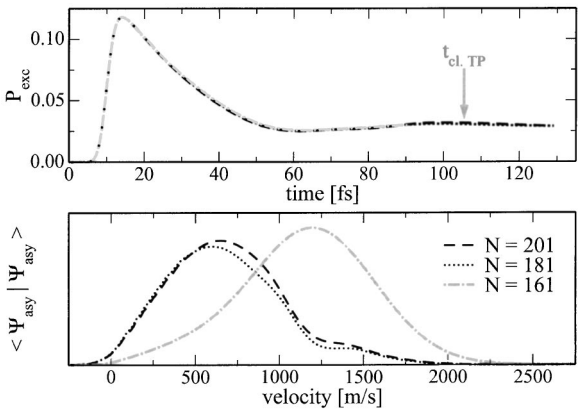

FIG. 11. The gray curves from Fig. 10 are plotted here for increasing number of bath modes N. The appearance of the high velocity peak is related to the passage of the classical turning point, but is independent of the increase in excited state population, i.e., it is not caused by the recurrences in the bath.

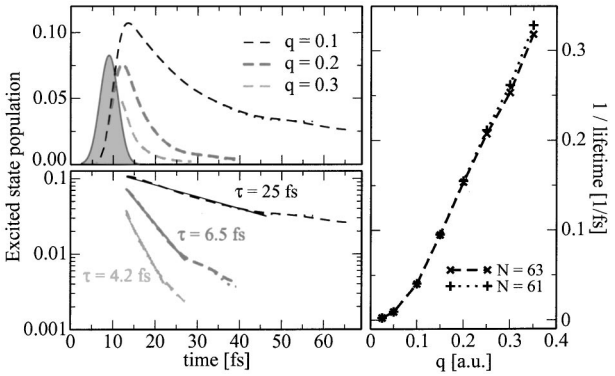

FIG. 12. The lifetime decreases with increasing dipole strength q ($N_L=1$).

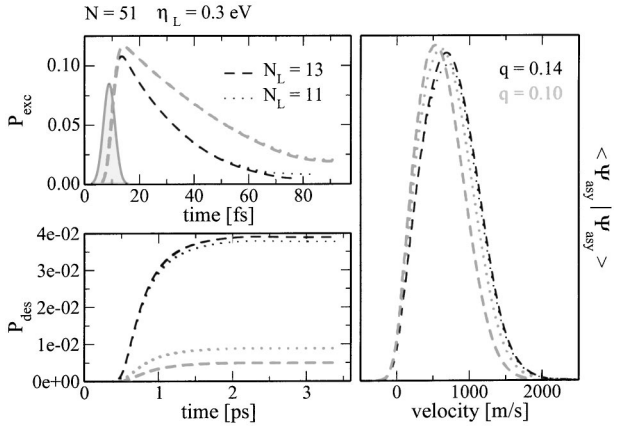

FIG. 13. The dipole strength q determines the lifetime (top left) and it leads to a very slight shift in mean velocity (right). The desorption probability was converged well enough to give an order of magnitude estimation (bottom left).

a single peak. For $N=181$ and $N=201$ modes, the excited state propagation continued beyond the classical turning point. Consequently, the velocity distributions exhibit an interference pattern. In particular, it can be concluded from Fig. 11 that the interferences in the velocity distributions appear independent from the population backflow since the latter is observed for all three cases presented in Fig. 11. Such interference can also be observed with the population backflow criterion—given that the propagation proceeded long enough on the electronically electronic state to pass the classical turning point. This was the case, for example, if an unphysically small TLS energy ε was chosen (cf. the solid curves in Fig. 4). The conclusion is that the interference pattern is not caused by recurrences in the bath, but it can unequivocally be related to the excited state dynamics.

E. Dependence on the dipole charge

There is only one parameter which enters the interaction Hamiltonian, Eq. (10), and the interaction constants, Eq. (11)—the dipole charge q. It characterizes the completeness of charge transfer between a nickel and an oxygen atom, $0 \leqslant q \leqslant 1$, and it determines the system–bath interaction strength. The dynamics can therefore be expected to depend crucially on q. Its value is related to the electronic structure of the substrate.

Figure 12 shows that an increase in q leads to a stronger interaction between system and bath and therefore to a smaller lifetime of the excited state. But the excited state dynamics is influenced in a twofold way: Besides the exponential decay which can be observed after the pulse has been applied, the maximum population of the excited state is decreased. The two phenomena are, of course, related. The latter, however, gives q the meaning of a parameter characterizing a metal to insulator transition, albeit in a very simplified way. For large q, no significant population of the excited state is observed at all. This corresponds to the case of metals where a direct optical excitation is immediately quenched due to the strong interaction with the substrate.

The exponentially decaying part of the excited state population versus time can be fitted to obtain decay rates or lifetimes. The fit is indicated for three examples in the lower left panel of Fig. 12 (solid lines). The obtained decay rates versus q are plotted in the right panel of Fig. 12. For $q \geqslant 0.1$, a linear dependence is observed. This corresponds to the coupling constants, Eq. (11), being linear in q.

The lifetime of the electronic state was estimated as about 25 fs.[5,42] With the surrogate Hamiltonian, such a lifetime is obtained for a comparatively small value of $q \approx 0.1$. A value of this order of magnitude seems justified, however, by the following consideration: The O $2p$ states are quite delocalized. One nickel atom therefore receives the electron from all its five or six neighboring oxygen atoms. But only the one or two charge transfer states with dipole moment parallel to the surface normal contribute to the dipole–dipole interaction. This gives a rough estimate of $0.15 \lesssim q \lesssim 0.2$. A similar number has been obtained independently in a population analysis of the O $2p \rightarrow$ Ni $3d$ charge transfer states obtained in electronic structure calculations.[63]

The lifetime of the electronically excited state and therefore q determine the desorption probability. While this is not confirmed by Fig. 13 (lower left panel) due to the convergence problem explained in the previous section, it can be observed in Fig. 14. Figures 13 and 14 have been obtained with the population backflow versus the bath distance criterion for switching off the bath. The desorption probability of $P_{\mathrm{des}} \approx 0.005-0.01$ for $q=0.1$ (gray line in Fig. 13) is too

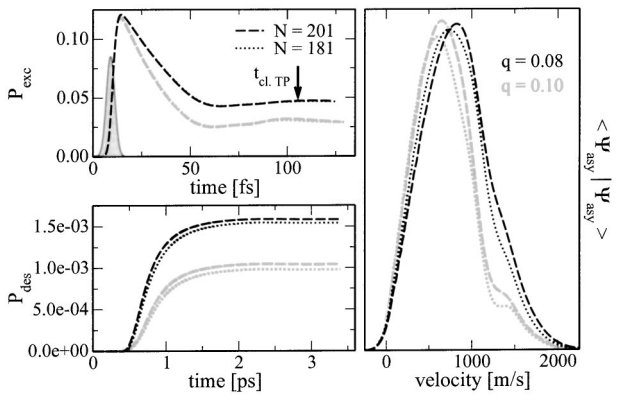

FIG. 14. The same as Fig. 13 (q varied), but with bath distance switch-off criterion. The velocity distributions have been scaled for comparison.

small because a comparatively large amount of population is neglected when switching off the bath. If the amount of neglected population is added to the desorbed norm, an upper limit for the desorption probability of about $P_{\mathrm{des}}=0.2$ is obtained. For $q=0.14$ (black line in Fig. 13), the observed desorption probability of about 4% is in the correct order of magnitude. In this case, the amount of neglected population was much smaller than for $q=0.1$. While the bath distance criterion leads to a higher desorption probability for smaller q as expected, it leads to a trapping of population on the excited state which does not seem to be physical. One could argue that the excited state population does not have to decay in an overdamped way, i.e., purely exponentially. This would lead to additional, decaying oscillations in the excited state population due to multiple electronic transitions. It is, however, beyond the current feasibility of the method to obtain convergence times long enough to test this hypothesis.

The desorption velocities (right panel of Figs. 13 and 14) depend only slightly on q. This is, however, subject to the convergence behavior. The shape of the velocity distributions might be changed considerably by the density which has been neglected when switching off the bath. While it seems reasonable to assume that all or most of the neglected population reaches the asymptotic region and desorbs, it is impossible to estimate with which velocities the desorption occurs. It should be pointed out, however, that in all cases the velocity distributions show intensity in the experimentally observed velocity range, and the desorption probability is of the expected order of magnitude for $q=0.14$, i.e., for a value of q close to the estimate from electronic structure calculations.

F. Dependence on the pulse parameters

A characteristic result of femtosecond photodesorption experiments has been the observation of a nonlinear dependence of the desorption yield or probability on the laser fluence. This indicates a DIMET mechanism and a fluence dependent transition from DIET to DIMET regimes.[64] Figure 15 therefore shows the dependence of the excitation quenching and the excited state decay on the laser fluence, i.e., $\int_{-\infty}^{\infty}E(t)dt$. The arrow in Fig. 15 indicates the pulse fluence which has been used in the remaining calculations. This value is still larger than the fluence of experimentally employed pulses (about 200 μJ in Ref. 41). The comparatively large value can be justified, however, to compensate for the simplification of just a single excited state which is accounted for in the theoretical model. This excited state is a representative of many, closely lying states which are in or close to resonance with the laser pulse in the experiment. The population transfer will therefore be higher than predicted by the model. This argument is supported by the independence of experimentally observed state resolved velocity distributions from the laser energy, $\hbar\omega_L$, which indicates a manifold of excited states with a very similar topology of their potential energy surfaces.[40] A similar conclusion has been reached by CI calculations.[4,5]

The excited state decay rate does not depend on the laser intensity (cf. Fig. 15). This is reasonable since the decay is caused by the substrate. For weak to moderate pulses, the

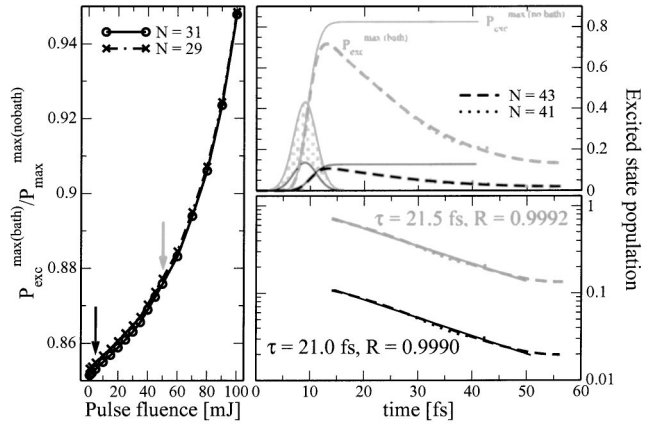

FIG. 15. Dependence of excitation quenching on pulse fluence: energies leading to about 10% excited state population as employed in the other calculations are in the linear regime (indicated by an arrow). The bath parameters are $\varepsilon=4$ eV, $\eta=2$ eV with resonant system excitation at $\omega_L=3.7$ eV and a pulse duration of $\tau_{\mathrm{FWHM}}=5$ fs. The excited state lifetime is not affected by increasing the pulse energy. The quality of the exponential fit is denoted by the correlation coefficient R.

excitation quenching (left panel of Fig. 15) shows a linear dependence on the fluence. For strong pulses, Rabi cycling between the two electronic states becomes significant leading to a nonlinear dependence. These intensities are very high, and Rabi cycling is probably insignificant. It was furthermore shown in a simulation without bath, that Rabi cycling has no influence on the desorption. In that case the population transfer is solely caused by the coupling to the laser pulse. The time spent on the excited state, however, turned out to be insufficient for desorption—independent of pulse intensity and length. Since Rabi cycling is the only mechanism in the present model, which can lead to a nonlinear dependence of the desorption probability on the fluence, it is not surprising that DIMET cannot be observed. DIMET can inevitably only be modeled by taking into account substrate-mediated excitation described by $\hat{\mathbf{H}}_{BF}(t)$.

The dependence of observables on the pulse duration is shown in Figs. 16 and 17. The lifetime of the excitation is also independent of pulse duration. This is expected and can be explained by the same argument as above: The decay is

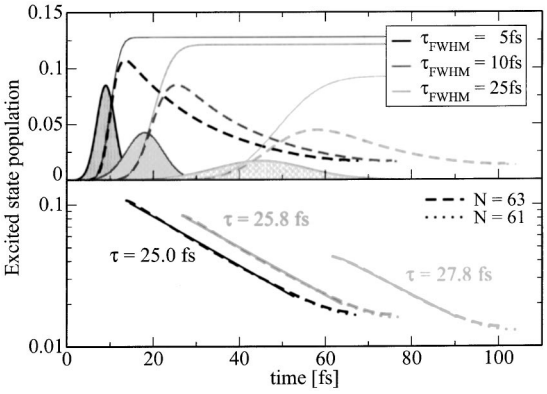

FIG. 16. The lifetime of the excitation is independent of pulse duration. The bath parameters are $\varepsilon=4$ eV, $\eta=2$ eV and the excitation is resonant at $\omega_L=3.7$ eV.

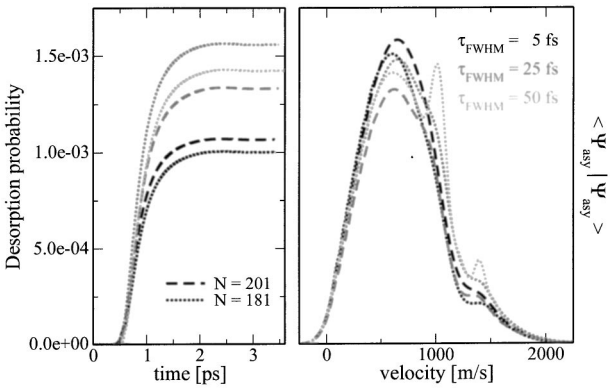

FIG. 17. Desorption probability and velocity distributions for varied pulse duration. Interference phenomena can be observed when the time scales of the pulse and of the nuclear dynamics become comparable.

caused by the substrate, and its rate should not be altered by the pulse. The independence of the decay rate from the pulse parameters points to a consistent treatment of the excitation process in the model. The excitation quenching, however, is influenced by the pulse FWHM—a longer pulse leads to an increased quenching (cf. Table II and Fig. 16). The system interacts simultaneously with the field and the bath. Therefore, in case of a larger FWHM and hence a longer interaction with the field, more population can be quenched.

The time in which the system simultaneously interacts with the field and the bath should furthermore influence the asymptotic observables. This is shown in Fig. 17. The results are, however, only preliminary due to the convergence problem discussed earlier. When the pulse duration becomes comparable with the vibrational period of the wave packet on the excited state potential, an interplay between pulse and nuclear dynamics can be observed. A longer pulse duration excites partial wave packets at times further away from each other. This leads to more different pathways which occur as interference pattern in the velocity distributions (Fig. 17, right). While this is consistent within the model, some caution is advisable when drawing conclusions with respect to experiment. In the present treatment, electronic dephasing has been completely neglected. Electronic dephasing will certainly wash out some of the observed quantum coherences. This effect should become more pronounced as the pulse duration is increased. The quantum coherences will furthermore be attenuated in a higher dimensional description.

IV. CONCLUSIONS

This study was aimed at a theoretical description of laser induced desorption where all aspects of the problem are treated on the same level of rigor. Potential energy surfaces obtained from first principles were combined with a microscopic model of the interaction between the excited adsorbate–substrate complex and substrate electron hole pairs causing the finite lifetime. The picture is based on a simplified description of the electron hole pairs as a bath of dipoles, and a dipole–dipole interaction between system and bath. All parameters were connected to results from electronic structure calculations. This direct derivation of the coupling constants from first principles is different from the more common treatments based on a reduced description and harmonic baths.

TABLE II. The quenching of excitation is increased for longer pulses.

$P_{\text{exc}}^{\text{max(bath)}}/P_{\text{exc}}^{\text{max(no bath)}}$	$\tau_{\text{FWHM}}=5$ fs	$\tau_{\text{FWHM}}=10$ fs	$\tau_{\text{FWHM}}=25$ fs
$N=59$	0.8407	0.7053	0.4823
$N=61$	0.8403	0.7045	0.4822
$N=63$	0.8399	0.7038	0.4818

In this first attempt to study laser induced desorption with the surrogate Hamiltonian method, converged excited state dynamics could be obtained. The convergence of asymptotic observables proved to be more difficult. The convergence behavior with respect to the parameters of the method was characterized. As a fully quantum mechanical, and therefore coherent method, the surrogate Hamiltonian suggests that experimentally observed bimodality of velocity distributions can be caused by quantum interferences known as Stückelberg oscillations. The surrogate Hamiltonian treatment represents the first attempt to microscopically model the relaxation which subsequently leads to desorption. The only parameter entering the system–bath interaction was the dipole charge q. This parameter was estimated by considering the geometry and electronic structure of the substrate. The value obtained agrees very well with an estimate from CI calculations. The model leads to desorption probabilities in the same order of magnitude as the experiment and to final velocity distributions in the experimentally observed range.

The results obtained with the surrogate Hamiltonian method, in particular the shape of the velocity distributions of desorbing molecules, should be considered as preliminary since the convergence requires improvement. They suggest, however, that the experimentally observed bimodality can be explained by quantum interferences due to different pathways. A similar interpretation had been given in Ref. 65, albeit with a simplified treatment of the relaxation. An alternative reason was suggested within a two-dimensional stochastic wave packet treatment.[5,42] There, the experimentally observed bimodality was connected to a bifurcation of the wave packet on the excited state caused by the topology of the excited state potential energy surface. These two hypotheses could be tested by an experiment as well as theoretical studies which change the vibrational frequencies of the potential while leaving the chemistry invariant. This could be accomplished, for example, by using different isotopes of the NO molecule.

While in a MCWF approach the lifetime of the excited state is empirically chosen and adjusted to give the correct desorption probability, the surrogate Hamiltonian approach yielded expectation values in the right range for both experimental observables which can be captured within a one-dimensional treatment, the desorption yield and the desorption velocities, without any adjustable parameters. The exact shape of the velocity distributions could, however, not be reproduced. The restriction of the present model to one dimension is certainly a flaw. A two-dimensional stochastic wave packet treatment showed a better compatibility with

the experimental results, i.e., bimodal velocity distributions. A combination of two-dimensional *ab initio* potential energy surfaces with the microscopic treatment of the dissipation in the surrogate Hamiltonian therefore paves the way toward a complete quantum mechanical description of the experiment.

In future work, vibrational relaxation for the ground state dynamics should be included. This could be accomplished by employing a second bath modeling the surface phonons. Vibrational relaxation for the excited state dynamics is insignificant due to the difference in time scales. In contrast the ground state wave packet leaves the potential well on the time scale of picoseconds meaning that vibrational relaxation plays a role. Furthermore, the dynamical simulations of the surrogate Hamiltonian should be supplemented by a detailed *ab initio* calculation of the dipole charge of nickel oxide. While an estimate based on CI calculations has been given in Ref. 63, a more accurate investigation would further reduce the uncertainty of this parameter in the surrogate Hamiltonian approach. Additionally, it should be investigated in more detail whether a substrate-mediated excitation is feasible within the surrogate Hamiltonian. This would allow for a direct comparison of the currently applied direct and a purely substrate-mediated excitation mechanism, and it would permit a theoretical investigation of the DIET to DIMET transition.[64] A substrate-mediated, i.e., indirect excitation mechanism can be modeled by exciting the TLS by the laser pulse,

$$\hat{\mathbf{H}}_{BF}(t)=E(t)\sum_i \mu_i(\hat{\boldsymbol{\sigma}}_i^{\dagger}+\hat{\boldsymbol{\sigma}}_i). \tag{14}$$

Indirect excitation of the adsorbate has so far been treated semi-phenomenologically by the two-temperature model neglecting, for example, the nonthermal nature of excited electrons.[32,33] Another approach took into account the nonlinear optical response of the substrate treating, however, the interaction between substrate and adsorbate in a TD-SCF framework.[34,35] In contrast to these approaches, a surrogate Hamiltonian treatment would allow for a microscopic description of the interaction between laser pulse and surface electrons. It needs to be investigated, however, whether a comparatively small number of bath modes would be sufficient to model excitation *and* deexcitation of the system due to the bath, i.e., whether such an approach would be numerically feasible. While modeling substrate-mediated excitation will require some effort, the description of a two-pulse experiment with the direct excitation model as employed in this paper is comparatively straightforward within the surrogate Hamiltonian. It requires, however, the characterization of a third electronic state describing the NO molecule, an unbound electron and the positively charged surface.

ACKNOWLEDGMENTS

We would like to thank Roi Baer for fruitful discussions and Stephan Thiel for reading the manuscript. Financial support from the German–Israeli Foundation for Scientific Research and Development (GIF) and from the Deutsche Forschungsgemeinschaft (SPP 1093) is gratefully acknowledged. The Fritz Haber Center is supported by the Minerva Gesellschaft für die Forschung GmbH München, Germany.

APPENDIX: MAPPING THE TWO-DIMENSIONS OF THE BATH ONTO ONE DIMENSION

The electron hole pairs which make up the bath are assumed to be localized on single Ni–O pairs. Then the bath is two dimensional (2D) considering the uppermost layer of the NiO surface or three dimensional (3D) in case several layers are considered. However, only the distance of each electron hole pair from the NO molecule and the direction of its dipole moment are important. In a one-dimensional treatment of the primary system only electron hole pairs with dipole moments parallel or antiparallel to the surface normal contribute to the dipole–dipole interaction. Therefore the bath is effectively one dimensional.

The fact that NiO has cubic lattice structure can be used to develop an algorithm to map a 2D or 3D bath onto one dimension (the distance) and a sign (the direction of the dipole). In 2D, each Ni–O pair is located at a point of a quadratic lattice. The lattice points correspond to numbers n, $0 \leqslant n \leqslant N_B \in \mathbb{N}$, for which $n=i^2+j^2$ holds with $i,j=0,\ldots \in \mathbb{N}$. This means that all square numbers and sums of two square numbers need to be found to determine the lattice points. A theorem from number theory can be employed: Every integer can be factorized into prime numbers $p=2$, $p=4m+1$, and $p=4m+3$. If and only if all prime factors $p=4m+3$ of n occur an even number of times in the factorization, n is a sum of two square numbers. The distance of this lattice point to the origin (which is the site below the NO molecule) is then given by

$$\text{distance of TLS}=\sqrt{n}a_0 \tag{A1}$$

with a_0 half the lattice constant. The sign of the dipole moment is given by

$$\begin{aligned} &i+j \ \text{ even}\rightarrow +, \\ &i+j \ \text{ odd}\rightarrow -. \end{aligned} \tag{A2}$$

If n can be factorized into different pairs (i,j), the number of possible factorizations corresponds to the number of times this distance occurs,

$$\text{occurrence}=\text{Number of different } (i,j)\cdot 4, \tag{A3}$$

where the factor 4 accounts for fourfold symmetry. Since points which are connected by a 90° rotation are identified, the surface slab is mapped onto a sphere. The usual assumption of periodic boundary conditions corresponds to a mapping onto a torus and does not make use of four-fold symmetry.

The outlined algorithm allows one to map a 2D bath, namely the dipoles in the uppermost layer of Ni–O pairs, onto one dimension. If additional Ni–O layers shall be treated to account for transport into the surface, the simplest approach describes every layer as a separate bath (cf. Fig. 18). This means that all correlations between layers are neglected. For the NO/NiO(100) system this should not pose a serious restriction. From physical considerations, there is already one restriction on the correlations between layers: The

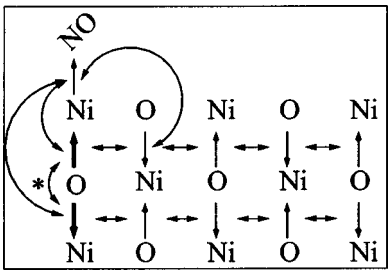

FIG. 18. Considering two layers of Ni–O pairs as two different baths: the system (bent arrows) interacts with each layer, the bath dipoles interact with each other within one layer (double arrows), the two layers are coupled by an interaction of dipoles on top of each other (bent arrow with an asterisk). For the system–bath interaction (bent arrows) and the interaction between different layers (bent arrow with an asterisk) only some representative arrows are drawn.

up and down dipoles marked in bold in Fig. 18 get excited by an electron transfer from the same oxygen atom, therefore it is very unfavorable that they are excited simultaneously. Analogously, it is unlikely that a nickel atom gets an electron from both the oxygen above and below. Therefore, this excitation can be excluded. So what really is neglected are the correlations between the down dipole marked in bold and all dipoles in the first layer and the correlations between the up dipole marked in bold and all dipoles in the second layer. Keeping in mind that so far only two to three simultaneous excitations within one layer needed to be allowed, this approximation should not be severe. It should be kept in mind that the approximation relies on the electronic structure of NiO, in particular on the localized *d*-orbitals. Thus this algorithm is not general, and the validity of the approximation might break down for other oxides, for example. However, then the whole ansatz of Eq. (9) might become questionable, for example, more than nearest-neighbor interaction should be included for a more delocalized electronic structure.

[1] H. Guo, P. Saalfrank, and T. Seideman, Prog. Surf. Sci. **62**, 239 (1999).
[2] R. Baer and R. Kosloff, J. Chem. Phys. **106**, 8862 (1997).
[3] C. P. Koch, T. Klüner, and R. Kosloff, J. Chem. Phys. **116**, 7983 (2002).
[4] T. Klüner, H.-J. Freund, J. Freitag, and V. Staemmler, J. Chem. Phys. **104**, 10030 (1996).
[5] T. Klüner, Ph.D. thesis, Ruhr-Universität Bochum, 1997.
[6] D. Menzel and R. Gomer, J. Chem. Phys. **41**, 3311 (1964).
[7] P. A. Redhead, Can. J. Phys. **41**, 886 (1964).
[8] P. R. Antoniewicz, Phys. Rev. B **21**, 3811 (1980).
[9] J. W. Gadzuk, L. J. Richter, S. A. Buntin, D. S. King, and R. R. Cavanagh, Surf. Sci. **235**, 317 (1990).
[10] J. Gadzuk, Surf. Sci. **342**, 345 (1995).
[11] M. Menges, B. Baumeister, K. Al-Shamery, H.-J. Freund, C. Fischer, and P. Andresen, J. Chem. Phys. **101**, 3318 (1994).
[12] J. W. Gadzuk, in *Laser Spectroscopy and Photochemistry on Metal Surfaces*, edited by H.-L. Dai and W. Ho (World Scientific, Singapore, 1995) pp. 897–942.
[13] W. T. Pollard, A. K. Felts, and R. A. Friesner, Adv. Chem. Phys. **93**, 77 (1996).
[14] V. May and O. Kühn, *Charge and Energy Transfer Dynamics in Molecular Systems* (Wiley-VCH, Berlin, 2000).
[15] R. Kubo, M. Toda, and N. Hashitsume, *Nonequilibrium Statistical Mechanics*, 2nd ed. (Springer, Berlin, 1991).
[16] P. Pechukas, Phys. Rev. Lett. **73**, 1060 (1994).
[17] G. Lindblad, Commun. Math. Phys. **48**, 119 (1976).
[18] V. Gorini, A. Kossakowski, and E. C. G. Sudarshan, J. Math. Phys. **17**, 821 (1976).
[19] R. Kosloff, M. A. Ratner, and W. B. Davis, J. Chem. Phys. **106**, 7036 (1997).
[20] N. Gisin and I. C. Percival, J. Phys. A **25**, 5677 (1992).
[21] C. W. Gardiner, A. S. Parkins, and P. Zoller, Phys. Rev. A **46**, 4363 (1992).
[22] R. Dum, A. S. Parkins, P. Zoller, and C. W. Gardiner, Phys. Rev. A **46**, 4382 (1992).
[23] M. B. Plenio and P. L. Knight, Rev. Mod. Phys. **70**, 101 (1998).
[24] P. Saalfrank, Chem. Phys. **211**, 265 (1996).
[25] P. Saalfrank, G. Boendgen, K. Finger, and L. Pesce, Chem. Phys. **251**, 51 (2000).
[26] T. Mančal and V. May, J. Chem. Phys. **114**, 1510 (2001).
[27] C. Meier and D. J. Tannor, J. Chem. Phys. **111**, 3365 (1999).
[28] R. P. Feynman and F. L. Vernon, Jr., Ann. Phys. (N.Y.) **24**, 118 (1963).
[29] N. Makri, Math Phys. **36**, 2430 (1995).
[30] N. Makri, Annu. Rev. Phys. Chem. **50**, 167 (1999).
[31] N. Makri, J. Phys. Chem. A **102**, 4414 (1998).
[32] P. Saalfrank and R. Kosloff, J. Chem. Phys. **105**, 2441 (1996).
[33] M. Nest and P. Saalfrank, J. Chem. Phys. **116**, 7189 (2002).
[34] Z. Yi, D. A. Micha, and J. Sund, J. Chem. Phys. **110**, 10562 (1999).
[35] D. A. Micha, A. Santana, and A. Salam, J. Chem. Phys. **116**, 5173 (2002).
[36] K. Mishima and K. Yamashita, J. Chem. Phys. **110**, 7756 (1999).
[37] T. Hertel, M. Wolf, and G. Ertl, J. Chem. Phys. **102**, 3414 (1995).
[38] D. H. Schirrmeister and V. May, Chem. Phys. Lett. **297**, 383 (1998).
[39] T. Mull, B. Baumeister, M. Menges, H.-J. Freund, D. Weide, C. Fischer, and P. Andresen, J. Chem. Phys. **96**, 7108 (1992).
[40] G. Eichhorn, M. Richter, K. Al-Shamery, and H. Zacharias, J. Chem. Phys. **111**, 386 (1999).
[41] C. Rakete, PhD thesis, Freie Universität Berlin (unpublished).
[42] T. Klüner, H.-J. Freund, V. Staemmler, and R. Kosloff, Phys. Rev. Lett. **80**, 5208 (1998).
[43] T. Klüner, S. Thiel, H.-J. Freund, and V. Staemmler, Chem. Phys. Lett. **294**, 413 (1998).
[44] G. Lindblad, J. Phys. A **29**, 4197 (1996).
[45] S. Thiel, T. Klüner, M. Wilde, K. Al-Shamery, and H.-J. Freund, Chem. Phys. **228**, 185 (1998).
[46] K. Blum, *Density Matrix Theory and Applications* (Plenum, New York, 1981).
[47] U. Weiss, *Quantum Dissipative Systems* (World Scientific, Singapore, 1993).
[48] N. V. Prokof'ev and P. C. E. Stamp, Rep. Prog. Phys. **63**, 669 (2000).
[49] A. O. Caldeira, A. H. Castro Neto, and T. Oliveira de Carvalho, Phys. Rev. B **48**, 13974 (1993).
[50] Y. Zhao, V. Chernyak, and S. Mukamel, J. Phys. Chem. A **102**, 6614 (1998).
[51] K. M. Forsythe and N. Makri, Phys. Rev. B **60**, 972 (1999).
[52] A. A. Golosov, S. I. Tsonchev, P. Pechukas, and R. A. Friesner, J. Chem. Phys. **111**, 9918 (1999).
[53] S. Thiel, M. Pykavy, T. Klüner, H.-J. Freund, R. Kosloff, and V. Staemmler, Phys. Rev. Lett. **87**, 077601 (2001).
[54] G. J. M. Jansen and W. C. Nieuwpoort, Phys. Rev. B **38**, 3449 (1988).
[55] H. Zacharias, G. Eichhorn, R. Schliesing, and K. Al-Shamery, Appl. Phys. B: Lasers Opt. **68**, 605 (1999).
[56] A. Leitheußer, Ph.D. thesis, Ruhr-Universität Bochum, 2001.
[57] H.-J. Freund, Faraday Discuss. **114**, 1 (1999).
[58] H. Kuhlenbeck and H.-J. Freund (private communication).
[59] F. Aryasetiawan and O. Gunnarsson, Phys. Rev. Lett. **74**, 3221 (1995).
[60] T. Klüner, H.-J. Freund, J. Freitag, and V. Staemmler, Mol. Catal. A: Chem. **119**, 155 (1997).
[61] R. Heather and H. Metiu, J. Chem. Phys. **86**, 5009 (1987).
[62] P. Saalfrank, Chem. Phys. **193**, 119 (1995).
[63] T. Klüner, Master's thesis, Ruhr-Universität Bochum, 1994.
[64] D. G. Busch and W. Ho, Phys. Rev. Lett. **77**, 1338 (1996).
[65] S. Thiel, T. Klüner, and H.-J. Freund, Chem. Phys. **236**, 263 (1998).